INSTITUTE OF PHYSICS PUBLISHING PHYSICAL BIOLOGY

Phys. Biol. **2** (2005) S86–S93 doi:10.1088/1478-3975/2/4/S02

Energy landscapes and properties of biomolecules

David J Wales

Department of Chemistry, Lensfield Road, Cambridge CB2 1EW, UK

E-mail: dw34@cam.ac.uk

Received 15 May 2005
Accepted for publication 29 July 2005
Published 9 November 2005
Online at stacks.iop.org/PhysBio/2/S86

Abstract

Thermodynamic and dynamic properties of biomolecules can be calculated using a coarse-grained approach based upon sampling stationary points of the underlying potential energy surface. The superposition approximation provides an overall partition function as a sum of contributions from the local minima, and hence functions such as internal energy, entropy, free energy and the heat capacity. To obtain rates we must also sample transition states that link the local minima, and the discrete path sampling method provides a systematic means to achieve this goal. A coarse-grained picture is also helpful in locating the global minimum using the basin-hopping approach. Here we can exploit a fictitious dynamics between the basins of attraction of local minima, since the objective is to find the lowest minimum, rather than to reproduce the thermodynamics or dynamics.

1. Introduction

Sampling stationary points of the underlying potential energy surface (PES) provides a convenient way to coarse-grain calculations of both thermodynamic and dynamic properties in molecular science [1]. In particular, this approach is not subject to the problems of ergodicity-breaking encountered in conventional simulations, and it is usually possible to address kinetics on the experimental time scale.

The stationary points in question are configurations where the gradient of the potential energy vanishes, which are further classified according to their Hessian index, i.e. the number of imaginary normal mode frequencies that they possess. A formally exact global partition function is obtained by summing over contributions from local minima, where all the normal mode frequencies are positive (or zero):

$$Z(T) = \sum_{\alpha} Z_{\alpha}(T). \tag{1}$$

The individual $Z_{\alpha}(T)$ are often calculated using a classical harmonic approximation for the vibrational density of states. This superposition approach is at least 30 years old [1–8] and it has been implemented with both anharmonic and quantum corrections [1].

To address kinetics we must also determine the transition states that link the local minima; these are defined here as stationary points of the potential energy that possess a single imaginary force constant [9]. Individual rate constants for transitions between connected local minima can then be obtained using statistical rate theory [10–14], which is usually implemented using classical harmonic densities of states [1].

Practical implementations of this potential energy landscape view depend upon efficient techniques for characterizing the local minima and transition states. Locating the transition states is generally the most time-consuming part of such a study. However, it is now possible to treat large systems quite routinely using methods based upon hybrid eigenvector-following [1, 15, 16] and the doubly nudged-elastic-band approach [17].

Once a suitable connected database of stationary points has been constructed, a global kinetic analysis can be performed using master equation [18, 19] or kinetic Monte Carlo [20–23] techniques. Master equation approaches have also been applied to discretized lattice models of proteins [24–26] and secondary structure models of RNA [27]. It is also important to address the issue of sampling, since the number of stationary points generally grows exponentially with system size [5, 28, 29]. The discrete path sampling approach [1, 30, 31] described in section 4 provides a means to construct appropriate databases systematically for larger systems.

The basin-hopping approach to global optimization [32], which is a generalization of the 'Monte Carlo plus energy

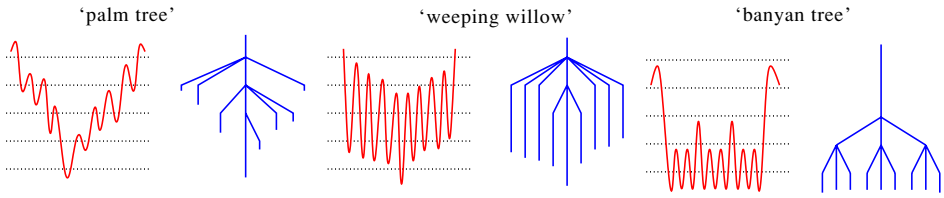

Figure 1. One-dimensional potential energy functions (left) and the corresponding disconnectivity graphs (right). The dotted lines indicate the energies at which a superbasin analysis was performed.

minimization' procedure of Li and Scheraga [33], is also based on coarse-graining the PES into the catchment basins of local minima. Here the moves between structures can be quite unrelated to pathways on the true PES, since the landscape is transformed in a way that removes transition state regions. This method is described in section 5, and the corresponding program `GMIN` can be downloaded from the internet along with other utilities for exploring the potential energy landscape [34].

2. Visualizing the PES using disconnectivity graphs

One of the most important themes in the present research is the question of how Nature has encoded the target structures for systems that are good 'structure seekers' in the potential energy landscape [35, 36]. This question links protein folding, crystallization, 'magic number' clusters in molecular beams and self-assembly processes. In each case the probability of finding the right structure in a random search is extremely small, and this is the essence of Levinthal's paradox from the field of protein folding [37]. In fact, the PES can effectively guide the system through the configuration space if the local minima are connected in the right way, and the resulting topology can be identified directly by constructing a disconnectivity graph [38–40]. This approach can also be generalized to discretized landscapes [41].

A connected database of local minima can be partitioned into disjoint sets, or 'superbasins', at any given total energy, E, where the members of each set can all be interconverted by one or more rearrangements without exceeding E. This basin analysis is performed at a series of energies, $E_1 < E_2 < E_3 < \cdots$, and each distinct superbasin is represented as a point, or node, on the horizontal axis. The vertical axis corresponds to the potential energy, and lines are drawn upwards starting from the potential energy of each local minimum, which is joined to the node for the superbasin in which it lies at the next energy level. Lines are drawn between nodes at adjacent levels if they correspond to the same superbasin or to superbasins that merge together.

Disconnectivity graphs are connected, but contain no cycles (they split into two parts if any edge is cut), and they are therefore classified as tree graphs. Three archetypal examples are shown in figure 1 [1, 39]. The 'palm tree' motif corresponds to a well-defined global minimum and relatively small downhill barriers, while the 'willow tree' pattern occurs when the barriers are larger, as for C_{60} [39, 42]. Finally, the 'banyan tree' landscape results when the connectivity exhibits a hierarchical pattern. In this case the hierarchy arises because local minima with similar potential energies are separated by barrier heights on two different energy scales (figure 1(c)). Cutting certain edges in such a structure disconnects whole sets of local minima in one go, in contrast to the palm tree and willow tree patterns.

Of course, the above motifs are idealizations, and quantitative calculations of thermodynamics and dynamics from stationary point databases do not depend upon the disconnectivity graph construction. Nevertheless, the qualitative behaviour of important observables may often be deduced from the form of the graph. In particular, the palm tree motif is associated with efficient relaxation to the global minimum over a wide range of temperature [1]. Such graphs can be viewed as a set of kinetically convergent pathways [43], which we may think of as a potential energy 'funnel', as discussed below. Free energy disconnectivity graphs can also be constructed by incorporating the entropy using appropriate vibrational densities of states for each stationary point, and by grouping sets of minima together [44–46].

A palm tree pattern is evident for the graph in figure 2, which corresponds to structures formed from 12 rigid pentagonal pyramids of height h and radius r [36]. This model was constructed to provide a simple representation of a virus capsid [47], and to determine minimal conditions on the pentamer–pentamer potential for self-assembly to occur spontaneously. Although each pentameric capsomer in a real virus, such as satellite tobacco necrosis virus, is actually composed of distinct protein subunits, there is some experimental evidence that the intra-capsomer binding is stronger than the interactions between capsomers [48, 49], providing a further level of simplification in the model. Theoretical studies also suggest that a pentagonal face may provide the best structure for nucleating capsid growth [50].

The formation of a closed icosahedral shell in figure 2 is entirely encoded within the six-site capsomer–capsomer potential [36]. Without a repulsive site at the apex of the pyramid, the pentamers would simply aggregate with their faces aligned. However, self-assembly into an icosahedral shell is predicted to be favourable over a relatively wide range of h, so long as the building blocks are not too flat and not too spiky [36]. It is the palm tree form of the disconnectivity graph that ensures this property, since the global potential energy minimum is also the global free energy minimum over a wide range of temperature where the system has sufficient thermal energy to overcome the potential energy barriers involved in relaxation from higher energy. By choosing an order parameter that reflects the distance from the global minimum, the potential energy 'funnel' may be projected onto a free

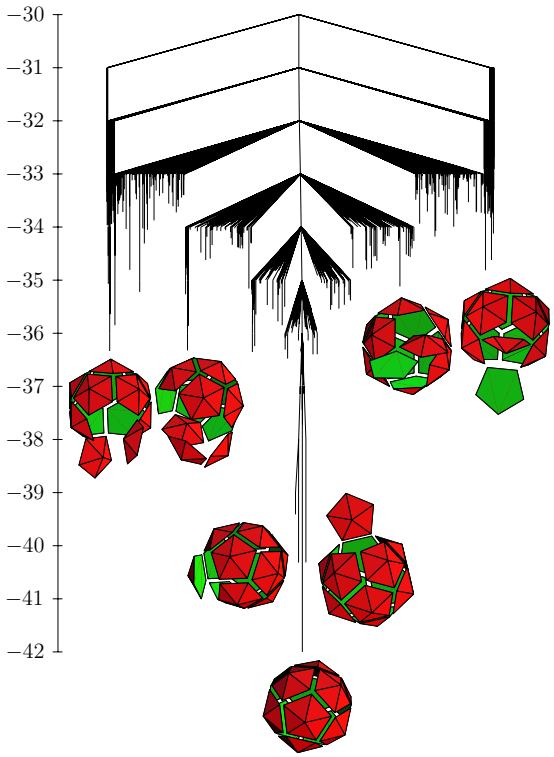

Figure 2. Disconnectivity graph for 12 pentagonal pyramids with $h = 0.5 \times r$. To simplify the graph, only the lowest 2000 local minima are shown, although all the minima were included in each superbasin analysis.

energy funnel, providing a link with theories based upon the random energy model and minimal frustration [51–55]. The palm tree form is also likely to result in a large value for T_f/T_g, where T_f is the 'folding' temperature, below which the potential energy and free energy global minima coincide, and T_g is the 'glass' temperature, where relaxation slows beyond some given time scale [56]. When T_f/T_g is large the global free energy minimum will be kinetically accessible over a wide range of temperature [57–59]. This situation has been associated with cooperative folding transitions via a calorimetric criterion [60]. The structure in figure 2 may also provide a realization of the hierarchically ordered constraint space proposed by Thorpe within the framework of constraint theory [61–64].

The palm tree disconnectivity graph therefore provides a visualization of how non-random searches may result in protein folding, crystallization, self-assembly and 'magic number' phenomena. It is also noteworthy that the construction of virus capsids from identical building blocks may optimize the use of genetic information [65] and utilize the funnelling properties of the corresponding PES.

Surfaces that support more than one palm tree structure also exhibit important characteristics [1]. For example, such systems often display a separation of time scales for relaxation to the global minimum, because trajectories may lead directly into the corresponding funnel, or they may be trapped in funnels containing competitive low-energy structures. Such cases have been analysed in detail for atomic clusters [1], and a biological example is presented in the following section.

3. Landscapes and dynamics of peptides

Polyalanine peptides, Ac-$(ala)_n$-NHMe or ala_n, have been considered in a number of experiments and simulation studies [1, 66–68]. The disconnectivity graph for ala_8 calculated using the AMBER95 potential [69] and a distance-dependent

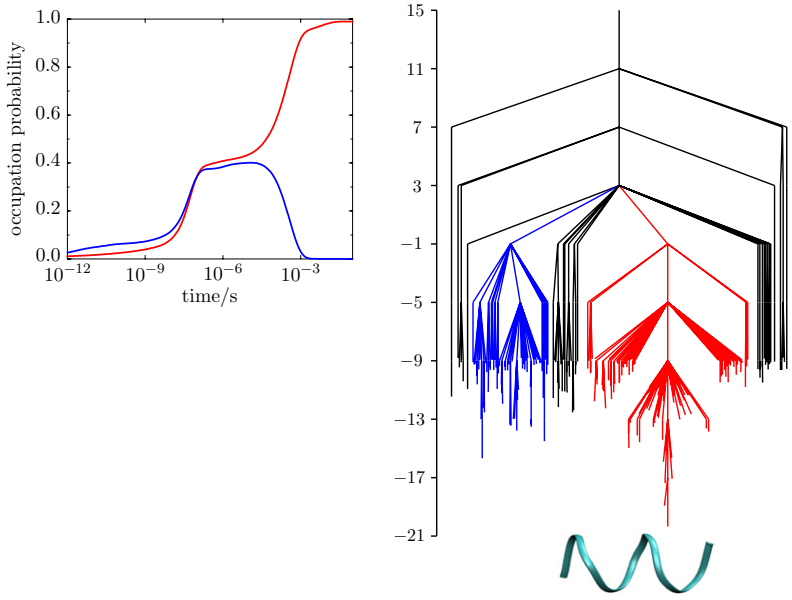

Figure 3. The disconnectivity graph for ala_8 calculated with the AMBER95 potential and a distance-dependent dielectric. The energy is in kcal mol^{-1}, and branches leading to minima with α and β character are coloured red and blue, respectively. On the left the occupation probability is plotted as a function of time starting from a high temperature equilibrium distribution.

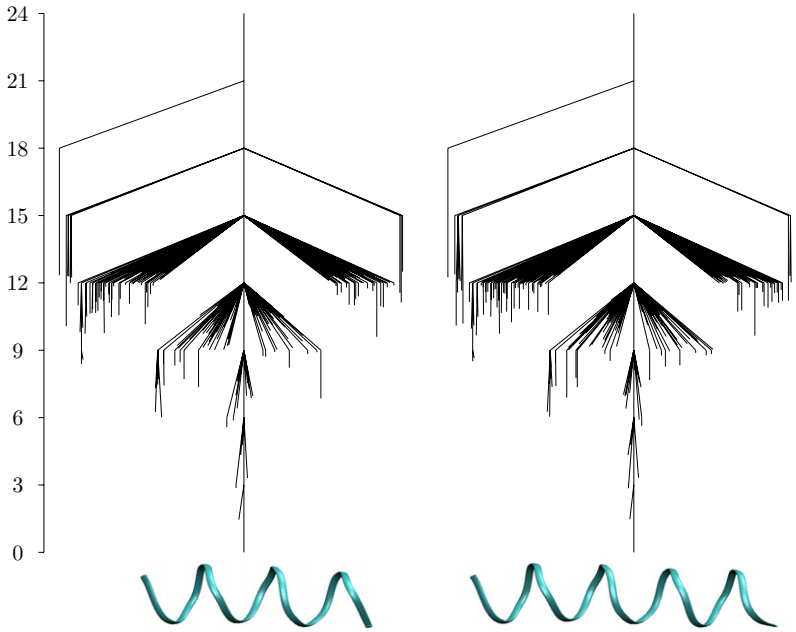

Figure 4. The disconnectivity graphs for ala_{12} (left) and ala_{16} (right) calculated with the AMBER95 potential and a distance-dependent dielectric. The energy is in kcal mol^{-1} relative to the global minimum.

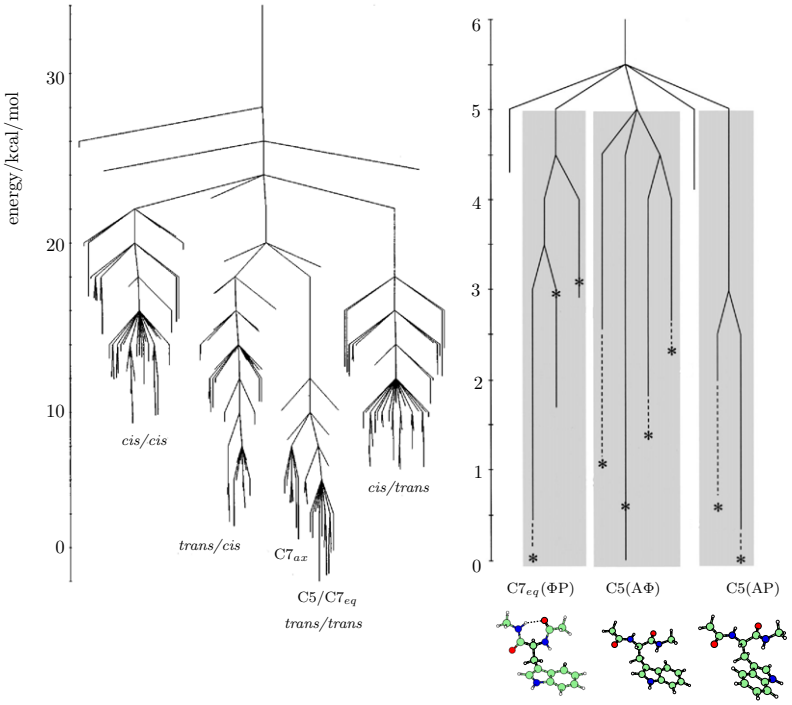

Figure 5. The disconnectivity graph for NATMA calculated using the AMBER95 force field (left) is compared with density functional theory (DFT) results (right) for the *trans*/*trans* isomers [72]. The DFT energetics are distinguished using dashed lines and asterisks.

dielectric as a crude representation of solvent is shown in figure 3 [70]. For this potential the dominant structure at 300 K was found to be predominantly helical, and this is probably an artifact of the distance-dependent dielectric. However, the disconnectivity graph and the corresponding relaxation dynamics shown in figure 3 serve to illustrate how two competing funnels result in a separation of relaxation time scales. A similar effect is seen in simplified lattice models of homopolymer and copolymer collapse, when suitable move sets are chosen to represent the dynamics [24–26].

The disconnectivity graphs calculated for ala_{12} and ala_{16} with the same potential are virtually superimposable at low

energy (figure 4) [71]. Helix formation was investigated by master equation dynamics in these peptides and was found to occur mainly from the ends [71], although these results are again strongly dependent upon the potential.

For smaller peptides, such as *N*-acetyl tryptophan methyl amide (NATMA), direct comparisons have been made between simulations and the conformational preferences determined spectroscopically [72]. Only three local minima with all *trans* peptide bonds are observed experimentally: C5 minima have extended structures, while $C7_{eq}$ minima exhibit seven-membered, hydrogen-bonded rings, which resemble a γ-turn. Barriers between the three shaded regions in figure 5 are relatively large, while the barriers within each region are smaller. Relaxation within each region is therefore relatively efficient, but transitions between the regions are slower, so that three minima are observed experimentally [72].

4. Discrete path sampling

The discrete path sampling approach [1, 30, 31] provides a systematic way to construct databases of stationary points that are appropriate for addressing dynamical properties. Here a discrete path is defined as a connected sequence of minima and the intervening transition state(s) between them, which provides a coarse-grained analogue of schemes based upon explicit dynamics [40, 75–88]. The final result is a database of local minima and transition states, which can then be subjected to kinetic analysis using master equation [18, 19] or kinetic Monte Carlo techniques [20–23, 89] to extract phenomenological rate constants [30, 31].

The most recent results for biomolecules involve the calculation of folding and unfolding rates for the neurotransmitter peptide met-enkephalin [73] and the 16-amino acid β hairpin-forming sequence from residues 41–56 of the B1 domain of protein G [74]. In each case the CHARMM19 force field [90] was used in conjunction with the EEF1 implicit solvation potential [91]. Results for met-enkephalin are shown in figures 6 and 7. Folding from extended conformations to a compact, low-energy II′-type β-turn structure occurs on a time scale of around 0.1 μs, while folding from a II-type β-turn structure has a calculated rate constant of $3.1 \times 10^7\ s^{-1}$ [73].

For the GB1 hairpin two kinetic intermediates were identified [74], in broad agreement with other studies [92–94]; the first is stable up to around 10^{-6} s and mainly consists of loosely hydrogen-bonded structures (F and G in figure 8). The second is dominant at around 10^{-5} s and consists of more compact structures, with a smaller radius of gyration for the hydrophobic core sidechains (C, D and E in figure 8). The calculated folding time is about ten times larger than experiment overall.

5. Basin-hopping global optimization

The basin-hopping global optimization approach [1, 32] is a generalization of the Monte Carlo plus minimization method of Li and Scheraga. The potential energy of a configuration $\mathbf{X}$

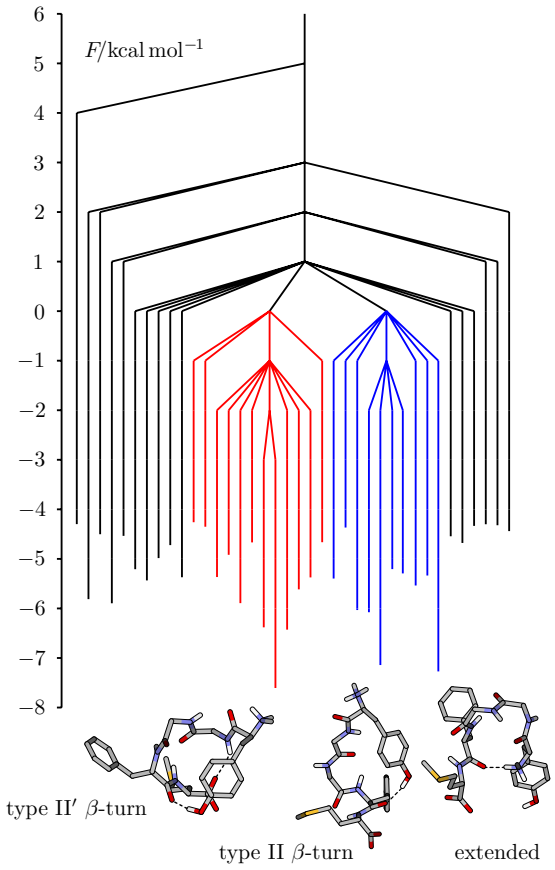

Figure 6. Free energy disconnectivity graph for met-enkephalin at 298 K. Each node represents a group of minima constructed as described in [73]. The lowest 38 groups are shown, as these are calculated to contain 90% of the population. The energy is in units of kcal mol^{-1} and the low-energy region of the graph contains two funnels, highlighted in red and blue.

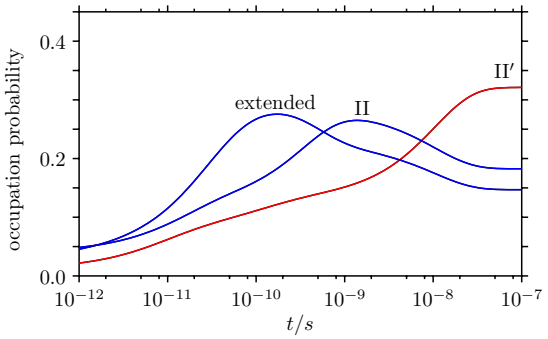

Figure 7. Results of master equation dynamics calculations for met-enkephalin at 298 K starting from a high temperature distribution (800 K) [73].

is transformed from the spontaneous value $V(\mathbf{X})$ to the value obtained after minimizing the energy, starting from $\mathbf{X}$:

$$\widetilde{V}(\mathbf{X}) = \min\{V(\mathbf{X})\}. \tag{2}$$

The transformed landscape $\widetilde{V}(\mathbf{X})$ consists of plateaux for the catchment basins of all the local minima, thus removing

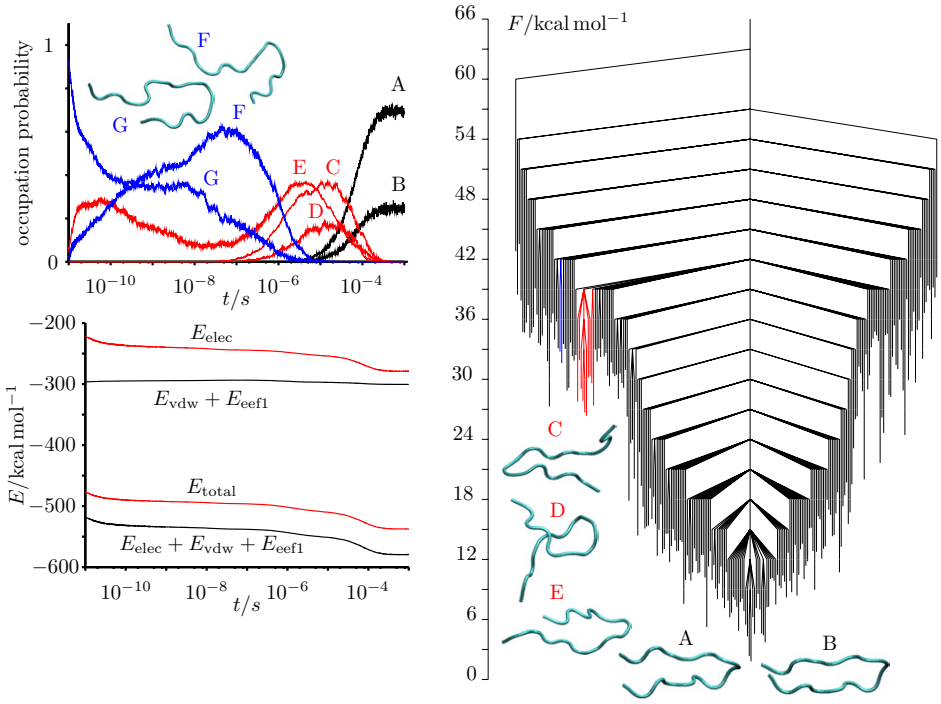

Figure 8. Free energy disconnectivity graph for the GB1 hairpin at 298 K [74] (right). The panel at the top left shows the time dependence of the occupation probability for various groups of minima, with a typical member of each set illustrated. The panel at the bottom left shows the average time dependence of different components of the potential energy [74]. E_{total} is the total potential energy, E_{elec} is the electrostatic energy, E_{vdw} is the van der Waals energy and E_{eef1} is the EEF1 solvation potential.

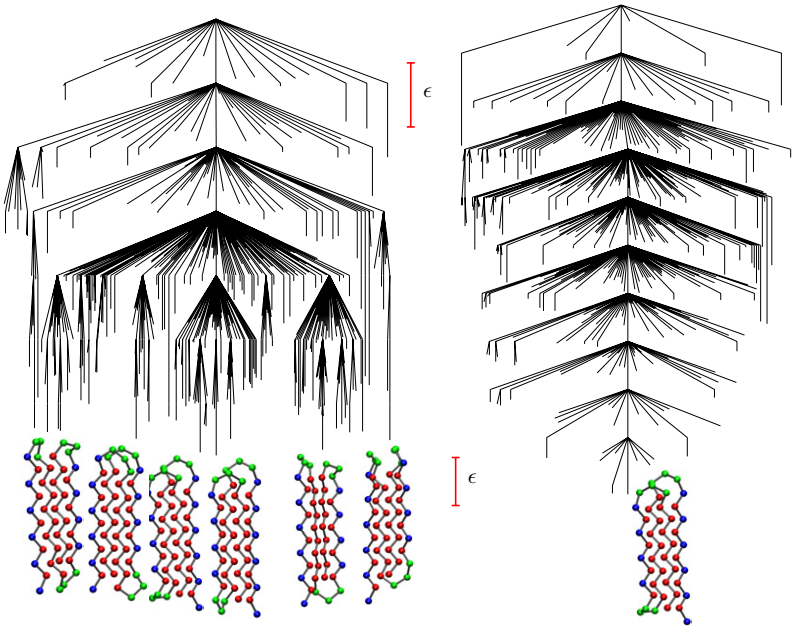

Figure 9. Disconnectivity graphs for the original (left) and Gō (right) BLN potentials.

all downhill barriers without changing the relative energies. Transitions between catchment basins can occur at any point along a boundary, while the occupation probabilities for different morphologies are broadened [95]. The basin-hopping approach has recently been applied to the BLN off-lattice bead model of Honeycutt and Thirumalai [96]. The original sequence of beads was $B_9N_3(LB)_4N_3B_9N_3(LB)_5L$, where B = hydrophobic, L = hydrophilic and N = neutral. The corresponding global minimum is a four-stranded β-barrel, which exhibits frustration in terms of alternative, low-lying β-barrel minima (figure 9). This frustration is relieved in the corresponding Gō model, which retains only the

attractive interactions present in the global minimum. The corresponding disconnectivity graph exhibits a palm tree form with a single potential energy funnel (figure 9) [97]. Conformational flow diagrams for native and Gō-like lattice models exhibit similar effects [26]. Introducing salt bridges into the potential [98] produces disconnectivity graphs with intermediate character [99]. The average number of basin-hopping steps required to locate the global minimum is largest for the original frustrated structure, smallest for the Gō model, and varies between these two limits for sequences with salt bridges, depending upon their location.

6. Conclusion

This brief overview is intended to show how a coarse-grained approach based on stationary points of the underlying potential energy surface (PES) can provide useful insight into biomolecular systems [1]. The methodology relies upon efficient geometry optimization techniques for locating and connecting the stationary points. Thermodynamic properties can then be calculated from a suitable sample of local minima using the superposition approach. The discrete path sampling method can be used to construct databases that include connectivity between local minima in terms of transition states of the PES. Dynamics on the experimental time scale may then become accessible if statistical rate theory is used to calculate the rate constants for transitions between connected local minima. Alternatively, to locate global minima the basin-hopping approach can be used, where Monte Carlo moves between local minima are accepted or rejected according to a Metropolis criterion. This method provides an algorithm that is readily transferable between very different systems.

References

[1] Wales D J 2003 *Energy Landscapes* (Cambridge: Cambridge University Press)
[2] McGinty D J 1971 *J. Chem. Phys.* **55** 580
[3] Burton J J 1972 *J. Chem. Phys.* **56** 3133
[4] Hoare M R 1979 *Adv. Chem. Phys.* **40** 49
[5] Stillinger F H and Weber T A 1984 *Science* **225** 983
[6] Franke G, Hilf E R and Borrmann P 1993 *J. Chem. Phys.* **98** 3496
[7] Wales D J 1993 *Mol. Phys.* **78** 151
[8] Wales D J, Doye J P K, Miller M A, Mortenson P N and Walsh T R 2000 *Adv. Chem. Phys.* **115** 1
[9] Murrell J N and Laidler K J 1968 *J. Chem. Soc. Faraday Trans.* **64** 371
[10] Pelzer H and Wigner E 1932 *Z. Phys. Chem.* B **15** 445
[11] Wynne-Jones W F K and Eyring H 1935 *J. Chem. Phys.* **3** 492
[12] Eyring H 1935 *Chem. Rev.* **17** 65
[13] Evans M G and Polanyi M 1935 *Trans. Faraday Soc.* **31** 875
[14] Evans M G and Polanyi M 1937 *Trans. Faraday Soc.* **33** 448
[15] Munro L J and Wales D J 1999 *Phys. Rev.* B **59** 3969
[16] Kumeda Y, Munro L J and Wales D J 2001 *Chem. Phys. Lett.* **341** 185
[17] Trygubenko S A and Wales D J 2004 *J. Chem. Phys.* **120** 2082
[18] van Kampen N G 1981 *Stochastic Processes in Physics and Chemistry* (Amsterdam: North-Holland)
[19] Kunz R E 1995 *Dynamics of First-Order Phase Transitions* (Thun: Deutsch)
[20] Bortz A B, Kalos M H and Leibowitz J L 1975 *J. Comput. Phys.* **17** 10
[21] Gillespie D T 1977 *J. Phys. Chem.* **81** 2340
[22] Gilmer G H 1980 *Science* **208** 355
[23] Fichthorn K A and Weinberg W H 1991 *J. Chem. Phys* **95** 1090
[24] Chan H S and Dill K 1993 *J. Chem. Phys.* **99** 2116
[25] Chan H S and Dill K 1994 *J. Chem. Phys.* **100** 9238
[26] Chan H S and Dill K 1998 *Proteins: Struct. Funct. Gen.* **30** 2
[27] Wolfinger M T, Svrcek-Seiler W A, Flamm C, Hofacker I L and Stadler P F 2004 *J. Phys. A: Math. Gen.* **37** 4731
[28] Doye J P K and Wales D J 2002 *J. Chem. Phys.* **116** 3777
[29] Wales D J and Doye J P K 2003 *J. Chem. Phys.* **119** 12409
[30] Wales D J 2002 *Mol. Phys.* **100** 3285
[31] Wales D J 2004 *Mol. Phys.* **102** 891
[32] Wales D J and Doye J P K 1997 *J. Phys. Chem.* A **101** 5111
[33] Li Z and Scheraga H A 1987 *Proc. Natl Acad. Sci. USA* **84** 6611
[34] The `GMIN` program, along with other software for exploring and visualising potential energy surfaces, is available for download at http://www-wales.ch.cam.ac.uk/software.html
[35] Ball K D, Berry R S, Kunz R E, Li F-Y, Proykova A and Wales D J 1996 *Science* **271** 963
[36] Wales D J 2005 *Phil. Trans. R. Soc.* A **363** 357
[37] Levinthal C 1969 Mössbauer spectroscopy biological systems *Proc. Meeting (Allerton House, Monticello, IL, 1969)* ed P DeBrunner, J Tsibris and E Munck (Champaign, IL: University of Illinois Press) p 22
[38] Becker O M and Karplus M 1997 *J. Chem. Phys.* **106** 1495
[39] Wales D J, Miller M A and Walsh T R 1998 *Nature* **394** 758
[40] Czerminski R and Elber R 1990 *J. Chem. Phys.* **92** 5580
[41] Flamm C, Hofacker I L, Stadler P F and Wolfinger M T 2002 *Z. Phys. Chem.* **216** 155 (The third author of reference [7] in this paper should be D J Wales)
[42] Kumeda Y and Wales D J 2003 *Chem. Phys. Lett.* **374** 125
[43] Leopold P, Montal M and Onuchic J 1992 *Proc. Natl Acad. Sci. USA* **89** 8721
[44] Krivov S V and Karplus M 2002 *J. Chem. Phys.* **117** 10894
[45] Evans D A and Wales D J 2003 *J. Chem. Phys.* **118** 3891
[46] Komatsuzaki T, Hoshino K, Matsunaga Y, Rylance G J, Johnston R L and Wales D J 2005 *J. Chem. Phys.* **122** 084714
[47] Zlotnick A 2004 *Proc. Natl Acad. Sci. USA* **101** 15549
[48] Eiserling F A and Dickson R C 1972 *Annu. Rev. Biochem.* **41** 467
[49] Davis B D, Dulbecco R, Eisen H N and Ginsberg H S 1980 *Microbiology* 3rd edn (New York: Harper and Row)
[50] Hespenheide B M, Jacobs D J and Thorpe M F 2004 *J. Phys. Condens. Matter* **16** S5055
[51] Frauenfelder H, Sligar S G and Wolynes P G 1991 *Science* **254** 1598
[52] Bryngelson J D, Onuchic J N, Socci N D and Wolynes P G 1995 *Proteins: Struct. Funct. Gen.* **21** 167
[53] Onuchic J N, Luthey-Schulten Z and Wolynes P G 1997 *Annu. Rev. Phys. Chem.* **48** 545
[54] Wolynes P G, Onuchic J N and Thirumalai D 1995 *Science* **267** 1619
[55] Socci N D, Onuchic J N and Wolynes P G 1998 *Proteins: Struct. Funct. Gen.* **32** 136
[56] Socci N D, Onuchic J N and Wolynes P G 1996 *J. Chem. Phys.* **104** 5860
[57] Bryngelson J D and Wolynes P G 1987 *Proc. Natl Acad. Sci. USA* **84** 7524
[58] Goldstein R A, Luthey-Schulten Z and Wolynes P G 1992 *Proc. Natl Acad. Sci. USA* **89** 4918
[59] Karplus M and Sali A 1995 *Curr. Opin. Struct. Biol.* **5** 58
[60] Chan H S, Shimizu S and Kaya H 2004 *Methods Enzymol.* **380** 350
[61] Phillips J C 1979 *J. Non-Cryst. Solids* **34** 153
[62] Phillips J C and Thorpe M F 1985 *Solid State Commun.* **53** 699
[63] Jacobs D J, Rader A J, Kuhn L A and Thorpe M F 2001 *Proteins: Struct. Funct. Genet.* **44** 150

[64] Phillips J C 2004 *J. Phys.: Condens. Matter* **16** S5065
[65] Crick F H C and Watson J D 1956 *Nature* **177** 473
[66] Young W S and Brooks C L 1996 *J. Mol. Biol.* **259** 560
[67] Levy Y and Becker O M 1998 *Phys. Rev. Lett.* **81** 1126
[68] Levy Y, Jortner J and Becker O M 2001 *Proc. Natl Acad. Sci. USA* **98** 2188
[69] Cornell W D, Cieplak P, Bayly C I, Gould I R, Merz K W Jr, Ferguson D M, Spellmeyer D C, Fox T, Caldwell J W and Kollman P A 1995 *J. Am. Chem. Soc.* **117** 5179
[70] Mortenson P N and Wales D J 2001 *J. Chem. Phys.* **114** 6443
[71] Mortenson P N, Evans D A and Wales D J 2002 *J. Chem. Phys.* **117** 1363
[72] Dian B C, Longarte A, Mercier S, Evans D A, Wales D J and Zwier T S 2002 *J. Chem. Phys.* **117** 10688
[73] Evans D A and Wales D J 2003 *J. Chem. Phys.* **119** 9947
[74] Evans D A and Wales D J 2004 *J. Chem. Phys.* **121** 1080
[75] Huo S and Straub J E 1997 *J. Chem. Phys.* **107** 5000
[76] Voter A F 1997 *Phys. Rev. Lett.* **78** 3908
[77] Huo S and Straub J E 1999 *Proteins* **36** 249
[78] Dellago C, Bolhuis P G and Chandler D 1999 *J. Chem. Phys.* **110** 6617
[79] Elber R O R and Meller J 1999 *J. Phys. Chem.* B **103** 899
[80] Sørensen M R and Voter A F 2000 *J. Chem. Phys.* **112** 9599
[81] Passerone D and Parrinello M 2001 *Phys. Rev. Lett.* **87** 108302
[82] Dellago C, Bolhuis P and Geissler P L 2002 *Adv. Chem. Phys.* **123** 1
[83] Bolhuis P G, Chandler D, Dellago C and Geissler P L 2002 *Annu. Rev. Phys. Chem.* **53** 291
[84] Krivov S V, Chekmarev S F and Karplus M 2002 *Phys. Rev. Lett.* **88** 038101
[85] Elber R, Ghosh A and Cardenas A 2002 *Accounts Chem. Res.* **35** 396
[86] Straub J E, Guevara J, Huo S and Lee J P 2002 *Accounts Chem. Res.* **35** 473
[87] Pratt L R 1986 *J. Chem. Phys.* **85** 5045
[88] Elber R and Karplus M 1987 *Chem. Phys. Lett.* **139** 375
[89] Gillespie D T 1976 *J. Comput. Phys.* **22** 403
[90] Brooks B R, Bruccoleri R E, Olafson B D, States D J, Swaminathan S and Karplus M 1983 *J. Comput. Chem.* **4** 187
[91] Lazaridis T and Karplus M 1999 *Proteins: Struct. Funct. Genet.* **35** 133
[92] Wei G, Derreumaux P and Mousseau N 2003 *J. Chem. Phys.* **119** 6403
[93] Bolhuis P G 2003 *Proc. Natl Acad. Sci. USA* **100** 12129
[94] Krivov S V and Karplus M 2004 *Proc. Natl Acad. Sci. USA* **101** 14766
[95] Doye J P K and Wales D J 1998 *Phys. Rev. Lett.* **80** 1357
[96] Honeycutt J D and Thirumalai D 1990 *Proc. Natl Acad. Sci. USA* **87** 3526
[97] Miller M A and Wales D J 1999 *J. Chem. Phys.* **111** 6610
[98] Stoycheva A D, Onuchic J N and Brooks C L 2003 *J. Chem. Phys.* **119** 5722
[99] Wales D J and Dewsbury P E J 2004 *J. Chem. Phys.* **121** 10284